Water Research 291 (2026) 125182

Contents lists available at ScienceDirect

Water Research

journal homepage: www.elsevier.com/locate/watres

Simultaneous photochemical oxidation of As(III) and Mn^{2+}(aq) in the presence of hematite

Junyeong Choi [a], Donggeun Kim [a], Seung Soo Steve Lee [b], John D. Fortner [b], Yoon Myung [c], Yuanzhi Tang [d,*], Haesung Jung [a,*]

[a] Department of Battery and Chemical Engineering, Changwon National University, Changwon, Gyeongsangnam-do 51140, Republic of Korea
[b] Department of Chemical and Environmental Engineering, Yale University, New Haven, Connecticut 06520, United States
[c] Korea Institute of Industrial Technology, Advanced Energy Materials and Components R&D Group, Busan 46744, Republic of Korea
[d] School of Earth and Atmospheric Sciences, Georgia Institute of Technology, Atlanta, Georgia 30332, United States

HIGHLIGHTS

- As(III) and Mn2+(aq) adsorb onto distinct surface sites of hematite.
- Simultaneous photochemical oxidation of As(III) and Mn2+(aq) occurs both in solution and on the hematite surface.
- Heterogeneous photocatalytic oxidation of As(III) proceeds through reactive oxygen species and direct electron transfer pathways, facilitated by molecular oxygen or heterogeneously nucleated Mn oxides.
- Under natural sunlight, heterogeneous oxidation of As(III) on hematite primarily proceeds via photocorrosion of Mn oxides.

GRAPHICAL ABSTRACT

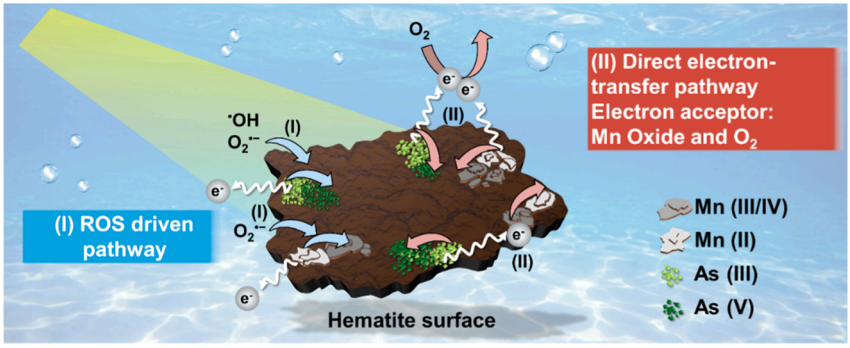

ARTICLE INFO

Keywords:
Simultaneous oxidation
Arsenic
Manganese
Hematite
Sunlight-driven photocatalysis

ABSTRACT

Arsenic (As), a toxic metalloid, is primarily released into natural aqueous systems through the reductive dissolution of Fe- and Mn-bearing minerals. Due to the frequent co-occurrence of Fe and Mn in As-contaminated surface waters and high redox reactivity of Fe and Mn oxides with As, Fe–As or Mn–As binary systems have been primarily investigated. However, the coupled redox interactions among all three elements under environmentally relevant conditions remain unclear. Here, we investigated the simultaneous photocatalytic oxidation of As(III) and Mn^{2+}(aq) in the presence of hematite under illumination. As(III) and Mn^{2+}(aq) adsorbed onto different surface sites of hematite, and underwent concurrent heterogeneous oxidation via reactive oxygen species and photocatalytic direct electron transfer. Notably, heterogeneously nucleated Mn oxides on hematite served as electron sinks, promoting the photocatalytic oxidation of As(III) through a photocorrosion mechanism. Outdoor sunlight experiments confirmed key findings observed under Xe-lamp conditions, including distinct adsorption behavior and concurrent oxidation of As(III) and Mn^{2+}(aq), validating the environmental relevance of the proposed mechanism. These findings provide novel insights into the redox cycling and fate of As in surface

* Corresponding authors.
E-mail addresses: yuanzhi.tang@eas.gatech.edu (Y. Tang), haesung.jung@changwon.ac.kr (H. Jung).

https://doi.org/10.1016/j.watres.2025.125182
Received 19 October 2025; Received in revised form 30 November 2025; Accepted 13 December 2025
Available online 15 December 2025

waters containing Fe and Mn, and suggest photocatalytic strategies for the simultaneous removal of As and Mn from contaminated environments.

1. Introduction

Arsenic (As), a naturally occurring toxic metalloid, is widely distributed in rocks, water, and plants. Exposure to As causes severe health effects, including neurological disorders, skin diseases, and cancer (Ramsay et al., 2021). In natural environments, As primarily enters surface waters and groundwater through the reductive dissolution of As-bearing minerals, such as iron sulfide, iron oxide, and manganese oxide (Chowdhury et al., 1999, Nickson et al., 1998). In aqueous systems, As primarily occurs as inorganic species (arsenite (As(III): H_3AsO_3 and $H_2AsO_3^-$) and arsenate (As(V): $H_2AsO_4^-$ and $HAsO_4^{2-}$) (Bednar et al., 2004), with concentrations typically below the World Health Organization guideline of 10 μg/L (Organization, 2022). However, elevated As levels, reaching hundreds to thousands of μg/L, have been reported in several regions, including Vietnam, China, and the United States, posing significant health risks (Ayotte et al., 2017, Winkel et al., 2011, Zhou et al., 2017). Moreover, recent studies have indicated that intensified droughts and floods resulting from climate change can alter water levels, triggering redox cycling and the reductive dissolution of As-bearing minerals, potentially increasing As mobilization (Lombard et al., 2021, Takahashi et al., 2004).

To mitigate the risks of As exposure, numerous studies have examined its fate and transport in natural aqueous systems. Since the use of contaminated groundwater is the most direct and critical exposure pathway, most studies have focused on subsurface systems (Nickson et al., 2000, Pi et al., 2024). However, surface water systems are also crucial because they are directly linked to food production and ecological health (Mondal et al., 2010). For instance, irrigation with As-contaminated surface water leads to As accumulation in rice grains, elevating dietary exposure (Abedin et al., 2002). Despite their importance, the redox behavior and mobility of As remain less studied in surface water systems than in groundwater systems, likely due to the more complex physicochemical processes occurring when As(III) interacts with surface water components such as oxygen, various environmental substances, and light.

Redox transformation is a key chemical process controlling As speciation, mobility, and toxicity, as As(III) is 25–60 times more toxic and mobile than As(V) (Bhandari et al., 2011, Mandal and Suzuki, 2002). The neutral charge of As(III) results in weaker adsorption onto mineral surfaces compared to that of the negatively charged As(V), making As(III) more mobile (Manning and Goldberg, 1997). Therefore, understanding the oxidation of As(III) is crucial in environmental geochemistry and remediation. Naturally occurring Mn and Fe oxides are recognized as effective oxidants of As(III) via direct electron transfer (Gude et al., 2017, Liu et al., 2021, Zhu et al., 2009). The oxidation of As (III) by Mn oxides ($MnO_2 + H_3AsO_3 + 2H^+ \rightarrow Mn^{2+} + H_3AsO_4 + H_2O$) is well documented, and Fe oxides have also been reported to oxidize As (III) (Manning et al., 2002).

Importantly, Fe, Mn, and As often co-occur in As-contaminated environments (Table S1), and Fe oxides, such as hematite, goethite, and ferrihydrite, readily nucleate in these systems, potentially facilitating ternary interactions among Fe oxides, Mn^{2+}(aq), and As(III) (Notini et al., 2022, Schwertmann et al., 1999). However, fundamental studies on their coexistence and interfacial behavior under environmentally relevant conditions remain limited (Bai et al. 2024). While engineered Fe–Mn binary oxides have been developed for As removal (Liu et al., 2022, Zhang et al., 2007), a fundamental understanding of their interactions under natural aqueous conditions remains lacking. Recently, studies from our group demonstrated that hematite, a ubiquitous natural Fe oxide, can photocatalytically oxidize Mn^{2+}(aq) under both simulated and natural sunlight, promoting the heterogeneous nucleation of Mn oxides on its surface (Choi et al., 2024, Jung et al., 2021). These findings suggest that hematite-driven photocatalysis can serve as a natural environmental pathway mediating the coupled oxidation of Mn^{2+}(aq) and As(III) in surface water systems.

In this study, we investigated the simultaneous photocatalytic oxidation of As(III) and Mn^{2+}(aq) in the presence of hematite under illumination. We demonstrated that As(III) and Mn^{2+}(aq) undergo concurrent oxidation on hematite surfaces while occupying different adsorption sites under xenon (Xe)-lamp conditions. We further explored the mechanistic pathways of this photocatalytic process and highlighted the role of hematite in mediating redox transformations of As(III) and Mn^{2+}(aq) under illumination. Finally, outdoor experiments under natural sunlight confirmed key observations, including distinct adsorption behaviors and concurrent oxidation, underscoring the relevance of the proposed mechanism for As and Mn cycling in sunlit aquatic environments. Our findings offer novel insights into the redox cycling and environmental fate of As in surface waters containing Fe and Mn, and suggest novel photocatalytic strategies for the simultaneous removal of As and Mn from contaminated systems.

2. Materials and methods

2.1. Preparation of hematite nanoparticles and artificial freshwater

Hematite nanoparticles were synthesized by following a previously reported procedure (Cornell and Schwertmann, 2003). X-ray diffraction (XRD; SmartlabSE, Rigaku) and field emission transmission electron microscopy (FE-TEM; JEM 2100F, Jeol) confirmed the formation of approximately 7 nm hematite nanoparticles (Choi et al., 2024, Jung et al., 2021). To simulate the natural sunlight-driven photocatalytic oxidation of As(III) and Mn^{2+}(aq) by hematite under freshwater conditions, artificial freshwater (AFW) was prepared. AFW contained 0.044 mM of $NaNO_3$, 0.448 mM of $MgSO_4$, 1.75 mM of $CaCl_2$, 0.0623 mM of $KHCO_3$, 0.0403 mM of KNO_3, and 1.1 mM of $NaHCO_3$ in deionized (DI) water (Ferris et al., 2004). The pH of AFW was 7.8 ± 0.1 and remained stable throughout the experiments.

2.2. Photochemical oxidation of As(III) and Mn^{2+}(aq) in the presence of hematite

Photocatalytic experiments were conducted at room temperature (25 °C) using a 300 W Xe-lamp (Newport). The light intensity was maintained at one sun (100 mW/cm^2), calibrated with a photometer (Power Meter Model 843-R, Newport). The reaction suspension was prepared by dispersing 0.10 g/L of hematite nanoparticles in 200 mL of AFW via sonication. $NaAsO_2$ (Duksan pure chemical) and $MnCl_2$ (Sigma Aldrich) were then added to achieve final concentrations of 133 μM As(III) and 100 μM Mn^{2+}(aq), respectively. These concentrations are within the range reported for polluted natural aquatic environments, where aqueous As can exceed 133 μM and Mn^{2+}(aq) frequently occurs in the range of 7.28–182 μM (Herath et al., 2016, Winkel et al., 2011). Photochemical reactions were performed in a 200 mL borosilicate reactor equipped with a vertical quartz window (diameter: 2.54 cm), facing the light source, and continuously stirred using a magnetic stir plate.

A dark control experiment was conducted by wrapping the reactor in aluminum foil to block light exposure. Aliquots of the reaction suspension were collected at designated time intervals. To quantify dissolved species, including total aqueous As, aqueous As(V), and Mn^{2+}(aq), the aliquots were filtered through a 0.2 μm PTFE syringe filter prior to analysis. The filtered samples were analyzed using an ultraviolet-visible

spectrophotometer (UV-Vis; Cary 60, Agilent) and inductively coupled plasma optical emission spectroscopy (ICP-OES; ICPE-9000, Shimadzu) (Jung et al., 2021, Lenoble et al., 2003). In contrast, total As(V) and Mn (III/IV) concentrations, including both dissolved and adsorbed/-nucleated species on hematite, were measured from unfiltered aliquots to assess the full extent of oxidation and precipitation of As and Mn. As (V) concentration was quantified using the molybdenum blue (MB) (Samchun chemicals) colorimetric assay at approximately 900 nm (Lenoble et al., 2003).

Mn(III/IV) concentration was analyzed using the leucoberbelin blue (LBB) (Sigma Aldrich) colorimetric method at 625 nm (Tebo et al., 2007). The reacted suspensions were mixed with MB and LBB at volume ratios of 5:1 and 1:5, respectively. The MB and LBB colorimetric assays used Na_2HAsO_4 (Sigma Aldrich) and $KMnO_4$ (Junsei Chemical) for standard calibration, respectively (Fig. S1). The concentration of oxidized Mn^{2+}(aq) was expressed as Mn(III) equivalents to represent the extent of electron transfer during Mn oxidation. This calculation was based on the stoichiometry whereby 1 mole of Mn(VII) oxidizes 5 moles of LBB (*i.e.*, 1 mole of oxidized LBB corresponds to the oxidation of 1 mole of Mn(II) to Mn(III)) (Choi et al., 2024, Jung et al., 2021). Dissolved Fe was measured by inductively coupled plasma optical emission spectroscopy (ICP-OES; ICPE-9000, Shimadzu). H_2O_2 was analyzed using titanium oxysulfate (Kanto chemical) colorimetric method at 410 nm (Eisenberg, 1943). The reacted suspensions were mixed with titanium oxysulfate reagent at volume ratios of 2:1. The titanium oxysulfate colorimetric assays used 30 % H_2O_2 (Daejung chemicals & metals) for standard calibration (Fig. S1).

The concentration of adsorbed As(V) onto hematite ($As(V)_{ads}$) was determined by subtracting the aqueous As(V) concentration ($As(V)_{aq}$) from the total As(V) concentration ($As(V)_{tot}$). All experiments were conducted independently in at least triplicate to ensure reproducibility. To elucidate the mechanism of the photochemical reaction, we conducted a series of control experiments, examining the roles of As(III), Mn^{2+}(aq), hematite, and light, as well as the electron transfer pathway and the Langmuir isotherm of As(III) and Mn^{2+}(aq). Detailed descriptions of the control experiments are provided in the Supporting Information (Text S1). The standard deviation of the $As(V)_{ads}$ concentration (σ_{ads}) was calculated using the error propagation ($\sigma_{ads} = \sqrt{(\sigma_{total})^2 + (\sigma_{aq})^2}$). At the conclusion of the experiments, solid products were collected using sequential centrifugation, washed twice with DI water, and freeze-dried. The freeze-drying process does not alter the oxidation states or crystalline structure (Hjorth, 2004). Detailed descriptions of the solid state analyses are provided in the Supporting Information (Text S2).

2.4. Photochemical oxidation of As(III) and Mn^{2+}(aq) in the presence of hematite under natural sunlight

The outdoor photocatalytic reactions were conducted on sunny days in July 2025, between 10 a.m. and 4 p.m., on the rooftop of the Second Engineering Building at Changwon National University (Changwon, Gyeongsangnam-do, South Korea; 35.2° latitude). The ambient temperature during the experiments was approximately 31.2 ± 1.2°C, and the intensity of natural sunlight was 64 ± 10 mW/cm^2, as measured with a photometer (Power Meter Model 843-R, Newport) on different dates and at different reaction times. For the experiments, hematite nanoparticles were suspended at 0.10 g/L in 50 mL of AFW and dispersed by sonication. $NaAsO_2$ and $MnCl_2$ were then added to obtain concentrations of 133 μM As(III) and 100 μM Mn^{2+}(aq) in the suspension. The photoreactions were conducted in a 100 ml borosilicate flask with continuous stirring under natural sunlight.

3. Results and discussion

3.1. Simultaneous oxidation of As(III) and Mn^{2+}(aq) in the presence of hematite under illumination

The simultaneous oxidation of As(III) and Mn^{2+}(aq) proceeded via photocatalytic reactions on hematite under light exposure (Fig. 1). After 6 h of light irradiation, approximately 47.6 ± 12.7 μM As(III) and 15.1 ± 2.6 μM Mn^{2+}(aq) were oxidized in the presence of hematite (Fig. 1A and B). While previous studies have primarily addressed the oxidation of As(III) by Mn oxides, coupled with the reduction of Mn oxides, our findings show the concurrent oxidation of As(III) and Mn^{2+}(aq). Control experiments conducted under dark conditions confirmed that the simultaneous oxidation of As(III) and Mn^{2+}(aq) occurred via a light-mediated pathway. Under dark conditions, the oxidized concentration of As(III) was approximately 8.7 ± 0.6 μM, significantly lower than that under light exposure (Fig. 1A). Similarly, the oxidation of Mn^{2+}(aq) was greater under light exposure (15.1 μM) than under dark conditions (8.9 μM), with the extent of oxidation increasing continuously over time (Fig. 1B). However, unlike As(III), Mn^{2+}(aq) exhibited only a marginal increase in oxidation under light exposure compared to dark conditions. The observed oxidation of Mn^{2+}(aq) on hematite under dark conditions occurred via the heterogeneous oxidation of Mn^{2+}(aq) by O_2 on hematite, as demonstrated in our previous studies (Jung et al., 2017a, Jung et al., 2021). Through the formation of a bidentate complex between adsorbed Mn(II) and two surface hydroxyl groups (>SOH), adsorbed Mn (II) undergo surface-mediated oxidation by O_2 (Diem and Stumm, 1984, Morgan, 2005).

Notably, under light exposure, the oxidation of As(III) occurred not only on the surface of hematite (*i.e.*, heterogeneous oxidation), but also in the solution (*i.e.*, homogeneous oxidation) (Fig. S2). After removing hematite from the illuminated suspension using a 0.22 μm syringe filter, we confirmed the presence of As(V) in the filtrate (Fig. S2A). Although the amount of As(V) on hematite was higher than that in the solution (Fig. S2A and S2B), the presence of As(V) in the filtrate indicated the occurrence of homogeneous oxidation. In contrast, under dark conditions, As(III) in solution remained unoxidized. These findings demonstrate that As(III) was oxidized to As(V) via both a photocatalytic heterogeneous pathway on the hematite surface and a photochemical homogeneous pathway in the aqueous phase.

To evaluate the role of Mn^{2+}(aq) in influencing the oxidation of As (III), we conducted a control experiment using only As(III) and hematite (Fig. S2C and S2D). Under light exposure, both heterogeneous and homogeneous oxidation of As(III) to As(V) occurred (Fig. S2). Furthermore, the overall photocatalytic oxidation of As(III) was greater in the absence of Mn^{2+}(aq) than in its presence for both oxidation pathways (Fig. S2E). This inhibitory effect of Mn^{2+}(aq) on As(III) oxidation was reciprocal (Fig. S2F). In the absence of As(III), the oxidation rate of Mn^{2+}(aq) was approximately 3.4 times higher than that observed in its presence after 6 h of reaction.

XPS analyses further confirmed the photocatalytic oxidation of both As(III) and Mn^{2+}(aq) on hematite (Fig. 1C). Under light exposure, the As 3d peak shifted to a higher binding energy compared to that under dark conditions, indicating the oxidation of As. Deconvolution of the As 3d spectrum showed that As(V) was the dominant species on hematite in the light-exposed sample, accounting for approximately 70 % of total As. In contrast, under dark conditions, As(III) predominated, comprising 86 % of total As, with only 14 % present as As(V) (Fig. S3).

For Mn, Mn(II) remained the predominant oxidation state on hematite under both light and dark conditions (Figs. 1C and S3). While previous studies have shown that Mn(III/IV) species dominate in Mn oxides formed via the photocatalytic oxidation of Mn^{2+}(aq) alone on hematite (Choi et al., 2024), the presence of As(III) altered this oxidation pathway, resulting in Mn(II) being the predominant oxidation state in the heterogeneously nucleated Mn oxides on hematite. Deconvolution of the Mn 3p spectrum showed that Mn(II) accounted for approximately 58

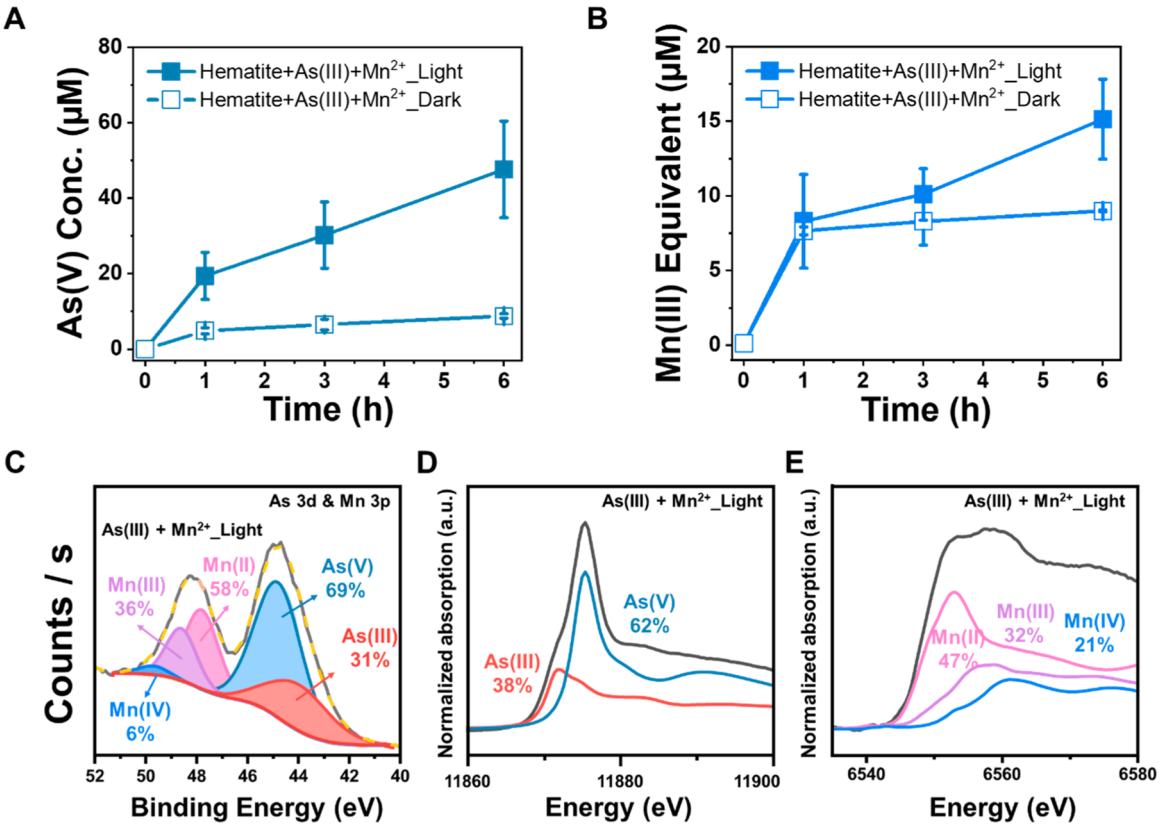

Fig. 1. Simultaneous photochemical oxidation of As(III) and Mn^{2+}(aq) by hematite. (A and B) Concentrations of As(V) and Mn(III) equivalent measured by colorimetric methods and inductively coupled plasma optical emission spectroscopy (ICP-OES) when As and Mn coexist with hematite under illuminated and dark conditions. (C) Deconvolution analysis of As 3d and Mn 3p X-ray photoelectron microscopy (XPS) spectra. (D and E) Linear combination fitting of As K-edge and Mn K-edge synchrotron-based X-ray absorption near edge structure (XANES) spectra, analyzing the oxidation states of As and Mn on hematite, respectively. The photochemical reaction was conducted with initial concentrations of 133 μM of As(III) and 100 μM of Mn^{2+}(aq) in the presence of 0.10 g/L of hematite.

% and 65 % of total Mn under light and dark conditions, respectively (Figs. 1C and S3). Although the Mn 3p deconvolution suggests a slightly higher Mn oxidation state under light exposure, this difference was not significant. Despite Mn(II) being dominant, XPS analysis confirmed the presence of Mn(III) and Mn(IV) species. Considering that Mn(III/IV) typically forms Mn oxides, we can infer that the nucleation of Mn oxides occurred on the hematite surface (Choi et al., 2024). However, due to the lower concentration of Mn oxide than hematite and the poor crystallinity of the nucleated Mn oxides compared to hematite, identifying the crystalline structure of the Mn oxides on hematite was challenging. XRD and TEM analyses confirmed no discernible differences in diffraction patterns or morphology between pristine hematite and reacted hematite (Fig. S4).

XANES analyses at the As K-edge and Mn K-edge further supported the XPS results. LCF indicated that As(V) and Mn(II) were the dominant oxidation states on hematite after reaction under light exposure, with As (V) comprising 62 % and Mn(II) comprising 47 % of the total species, respectively (Fig. 1D and E). Although a direct quantitative comparison between XANES (bulk-sensitive) and XPS (surface-sensitive) data is inherently limited due to differences in analytical depth and potential fitting uncertainties, the oxidation state distributions from both techniques were reasonably consistent.

3.2. *Difference in adsorption sites of As and Mn on hematite surface*

Our control experiments suggest that As(III) and Mn^{2+}(aq) occupy distinct adsorption sites on hematite (Fig. 2). Despite faster oxidation of both species under light than under dark conditions, the adsorbed amounts of As and Mn on hematite remained relatively constant across both conditions (Fig. 2A and B). After 6 h, the concentrations of the residual aqueous As species were 69.5 ± 2.8 μM and 77.5 ± 0.3 μM under light and dark conditions, respectively (Fig. 2A). Notably, when photocatalytic oxidation was performed using As(III) alone, without Mn^{2+}(aq), the amount adsorbed on hematite was similar to that observed in the presence of both As(III) and Mn^{2+}(aq) (Fig. 2A). Specifically, the concentrations of the residual aqueous As species in the presence and absence of Mn^{2+}(aq) were 69.5 ± 2.8 μM and 81.6 ± 1.4 μM, respectively. These results indicate that neither light nor Mn^{2+}(aq) significantly influenced the adsorption of As(III) on hematite. In particular, the similar adsorbed amounts of As(III) in the controlled tests imply that heterogeneously nucleated Mn oxides formed via photocatalytic oxidation of Mn^{2+}(aq) on hematite play a minor role in the adsorption of As.

In the presence of both As(III) and Mn^{2+}(aq) in solution, the aqueous Mn concentration after 6 h was 55.9 ± 5.3 μM and 61.7 ± 1.8 μM under light and dark conditions, respectively (Fig. 2B). In addition, under dark conditions, the adsorption of Mn^{2+}(aq) onto hematite was comparable regardless of the presence of As(III) (Fig. 2B). The aqueous Mn concentration in the absence of As(III) was 64.5 ± 3.9 μM, similar to that observed when As(III) was present. This result suggests that As(III) has minimal influence on the adsorption of Mn^{2+}(aq). Collectively, these results indicate that As(III) and Mn^{2+}(aq) occupy distinct adsorption sites on hematite.

Time-lapse addition experiments under dark conditions further support the presence of different adsorption sites for As(III) and Mn^{2+}(aq) (Fig. 2C and D). After 3 h of reaction with 133 μM As(III) and hematite, we added 100 μM Mn^{2+}(aq) and found that the aqueous As and Mn concentrations were 81.9 ± 5.6 μM and 67.1 ± 11.7 μM, respectively (Fig. 2C). Conversely, after 3 h of reaction with 100 μM Mn^{2+}(aq) and hematite, we added 133 μM As(III) and found that the

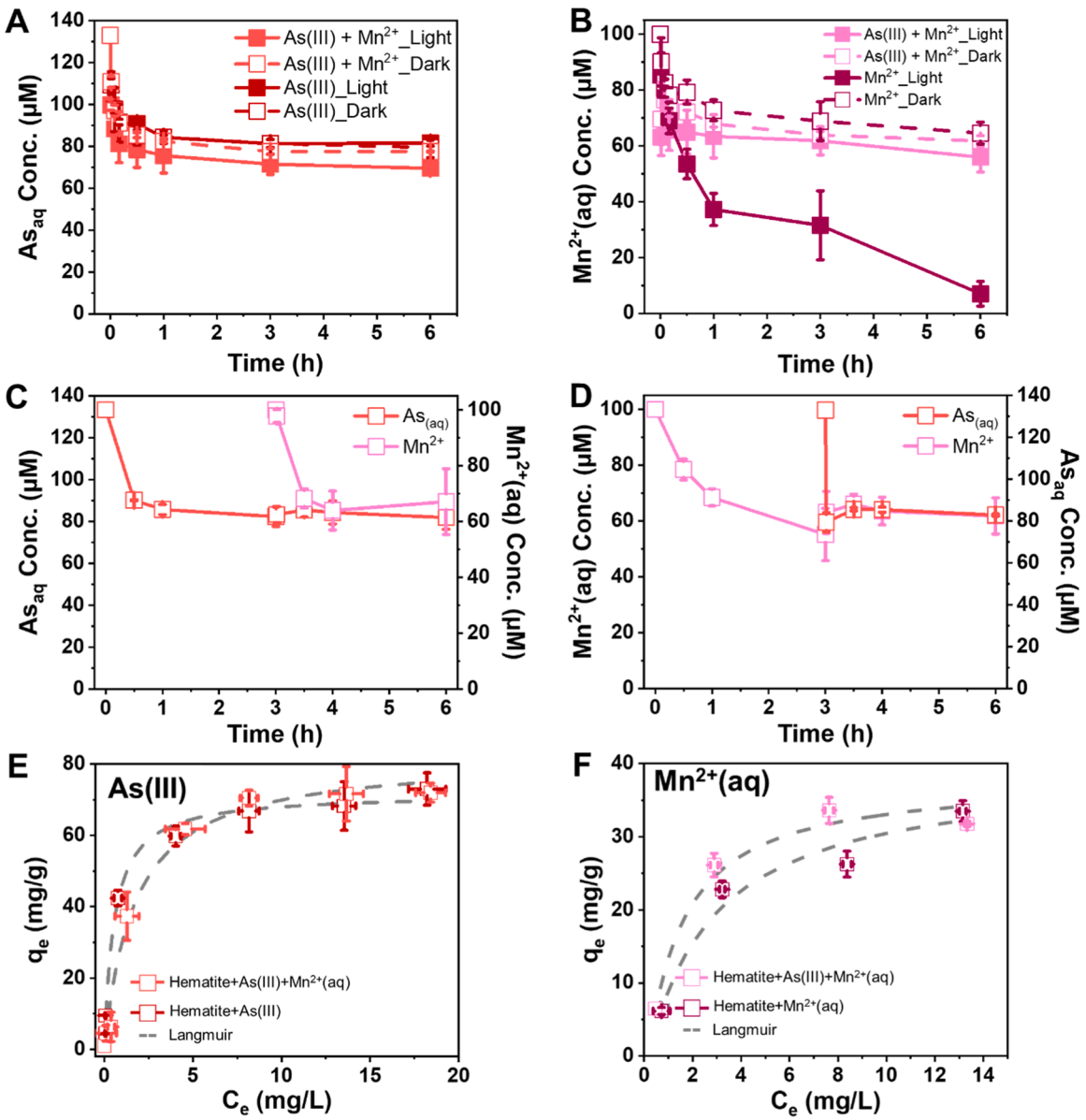

Fig. 2. Differences in the adsorption sites of As and Mn on hematite. (A and B) Concentrations of aqueous As and Mn^{2+}(aq) species. (C and D) Concentrations of aqueous As and Mn^{2+}(aq) species with time-lapsed addition of As(III) or Mn^{2+}(aq) under dark conditions. (E and F) Langmuir isotherms for the adsorption of As(III) and Mn^{2+}(aq) on hematite under dark conditions. The amount of adsorbed As on hematite remained consistent whether As was present alone or coexisting with Mn^{2+}(aq). Similarly, the adsorption of Mn^{2+}(aq) on hematite was largely unaffected by the presence or absence of As.

aqueous As and Mn concentrations were 82.8 ± 0.5 μM and 61.8 ± 6.4 μM, respectively (Fig. 2D). The consistent amounts of adsorbed As and Mn on hematite in both systems provide strong evidence that As(III) and Mn^{2+}(aq) occupy distinct adsorption sites.

Analysis of the Langmuir isotherms for As(III) and Mn^{2+}(aq) further corroborates the presence of distinct adsorption sites on hematite (Fig. 2E and 2F; Table S2). For As(III), the maximum adsorption capacity (q_{max}) remained quite similar with or without Mn^{2+}(aq) (Fig. 2E). When both As(III) and Mn^{2+}(aq) were present in solution with hematite, q_{max} for As(III) was 81.9 mg/g. In the presence of As(III) alone with hematite, q_{max} was 71.7 mg/g. These results suggest that the presence of Mn^{2+}(aq) has only a minor effect on the adsorption of As(III) onto the hematite surface. For Mn^{2+}(aq), the Langmuir isotherm showed consistent q_{max} value irrespective of the presence or absence of As(III) (Fig. 2F). When both As(III) and Mn^{2+}(aq) were present in solution with hematite, q_{max} for Mn^{2+}(aq) was 38.0 mg/g. In the presence of Mn^{2+}(aq) alone, q_{max} was 39.1 mg/g. Thus, combined with the analysis of soluble As and Mn^{2+}(aq) concentrations (Fig. 2A and B), the Langmuir isotherm data provided strong evidence for distinct adsorption sites of As(III) and Mn^{2+}(aq) on hematite.

3.3. *Homogeneous photochemical oxidation of As(III) and Mn^{2+}(aq)*

Under light conditions, simultaneous and rapid oxidation of As(III) and Mn^{2+}(aq) occurred via both homogeneous and heterogeneous pathways in the presence of As(III), Mn^{2+}(aq), and hematite. Control experiments demonstrated that homogeneous oxidation of As(III) and Mn^{2+}(aq) in solution was mediated by superoxide, one of the most reactive oxygen species (ROS) responsible for their oxidation (Fig. 3). In the presence of superoxide dismutase (SOD), the most widely used superoxide scavenger, the oxidation of As(III) decreased both in the filtrate and on hematite (Fig. 3A, B, and C). Similarly, the oxidation of Mn^{2+}(aq) decreased in the presence of SOD (Fig. 3D). However, the adsorption of aqueous As and Mn^{2+}(aq) was unaffected by SOD (Fig. S5).

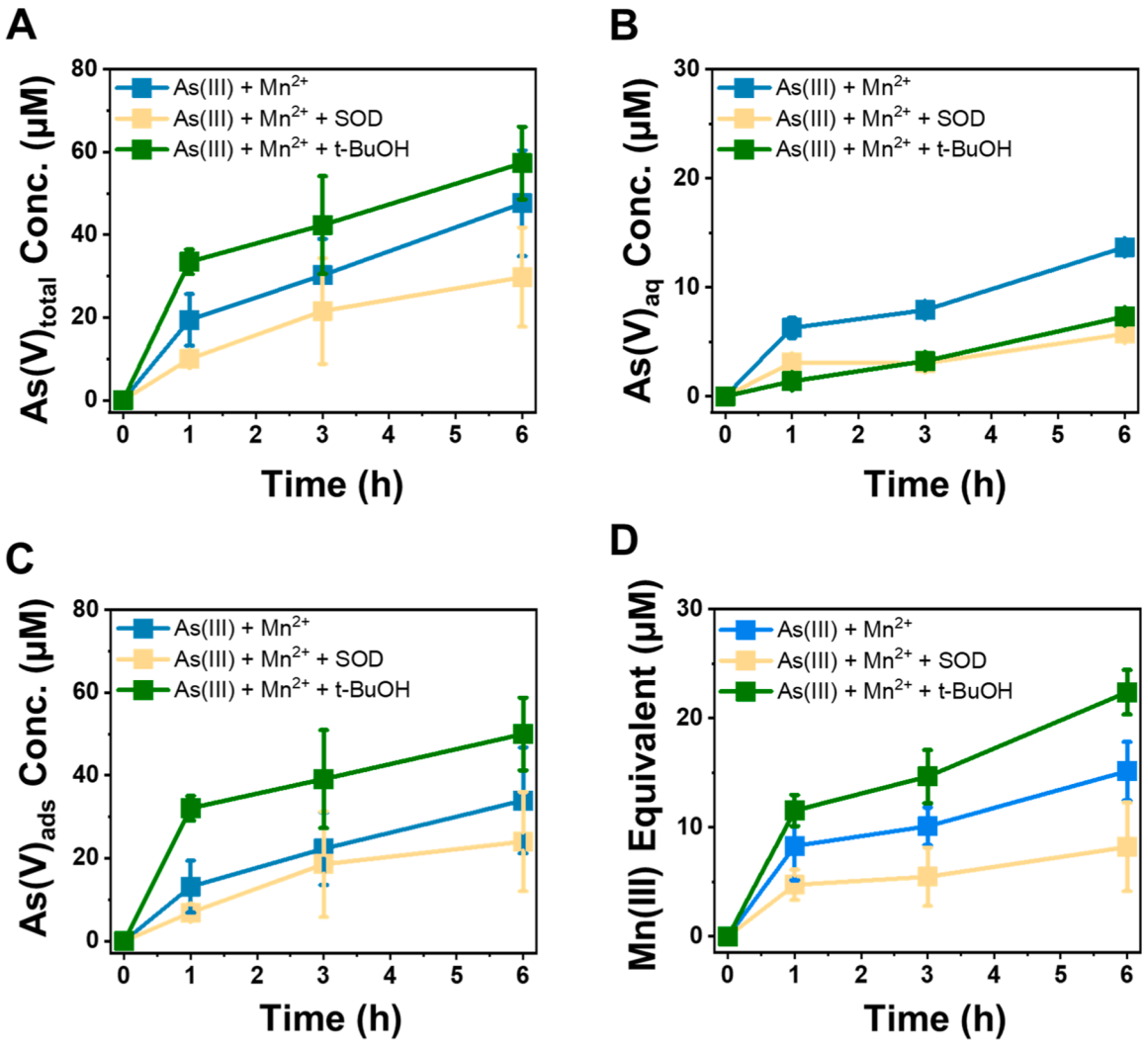

Fig. 3. Photochemical oxidation of As(III) and Mn^{2+}(aq) in the presence of hematite via reaction with reactive oxygen species (ROS). Concentrations of (A) total As (V), (B) aqueous As(V), (C) adsorbed As(V), and (D) Mn(III) equivalents in the presence or absence of ROS scavengers. The decreased concentrations of As(V) and Mn (III) equivalents in the presence of superoxide dismutase (SOD) suggest that superoxide, generated by the photoexcitation of nitrate, induces the oxidation of As(III) and Mn^{2+}(aq) both in solution and on hematite. In the presence of *tert*-butyl alcohol (t-BuOH) under illumination, enhanced oxidation of adsorbed As(III) on hematite occurred. Peroxyl radicals ($ROO^{\bullet}$), generated when t-BuOH scavenges hydroxyl radicals, accelerated the oxidation of Mn^{2+}(aq) and the subsequent nucleation of Mn oxide. This enhanced Mn^{2+}(aq) oxidation and Mn oxide formation likely promoted the oxidation of adsorbed As(III) on hematite. The initial concentrations used in the experiments were 133 μM of As(III), 100 μM of Mn^{2+}(aq), and 0.10 g/L of hematite with 0.5 μM of SOD or 0.1 M of t-BuOH.

Since the conduction band of hematite lies at a more positive potential than the O_2/superoxide redox couple, hematite cannot generate superoxide via band-gap excitation (Jung et al., 2021). Instead, superoxide is likely generated through direct photoactivation of As(III) or nitrate in AFW (0.044 mM of $NaNO_3$, and 0.0403 mM of KNO_3), both of which can yield superoxide under UV light irradiation (Table S3 and S4) (Kim et al., 2014, Ryu et al., 2013). To evaluate this hypothesis, we conducted a series of control experiments in the absence of hematite (Jung et al., 2021). Upon light exposure, a solution containing only As (III) and Mn^{2+}(aq) underwent simultaneous oxidation of both species (Fig. S6A and S6B), resulting in the oxidation of 23.0 ± 1.7 μM of As(III) and 3.6 ± 1.1 μM of Mn^{2+}(aq) after 3 h of reaction. Under dark conditions, oxidation was negligible.

Notably, in the absence of hematite, when SOD was added to the illuminated solution, oxidation of both As(III) and Mn^{2+}(aq) was completely suppressed (Fig. S6A and S6B), confirming superoxide as the primary oxidant. To evaluate whether Mn^{2+}(aq) influenced the homogeneous oxidation of As(III) by superoxide, we compared photochemical oxidation in the presence and absence of Mn^{2+}(aq) (Fig. S6A and S6C). The oxidation of As(III) was comparable under both conditions. Furthermore, when a 400 nm cut-off filter was used to inhibit the photoexcitation of As(III) or nitrate, and thereby reduce superoxide formation, the oxidation of As(III) was suppressed (Fig. S7A) (Kim et al., 2014, Ryu et al., 2013). To distinguish the species generating superoxide between As(III) and nitrate, we conducted experiments using nitrate-free AFW prepared by omitting nitrate sources, and observed the complete suppression of As(III) oxidation (Fig. S7B). These control experiments elucidate the significant role of superoxide generated by UV light driven nitrate photoexcitation in the homogeneous photochemical oxidation of As(III). Although the nitrate concentration in AFW was low (0.044 mM $NaNO_3$ and 0.0403 mM KNO_3), its photoexcitation induced the rapid oxidation of As(III). The photoexcitation of As(III) was likely less significant than nitrate because of negligible UV-C in Xe-lamp irradiation (Kim et al., 2014, Ryu et al., 2013).

We also confirmed the contribution of hydroxyl radicals to the homogeneous oxidation of As(III) (Fig. S6C). In illuminated solutions containing only As(III) and *tert*-butyl alcohol (t-BuOH), a well-known hydroxyl radical scavenger, the oxidation of As(III) was 12.7 ± 0.8 μM after 3 h, which is lower than in the absence of t-BuOH (27.1 ± 0.9 μM). This result indicates that hydroxyl radicals also contribute to the

homogeneous oxidation of As(III). The complete suppression of As(III) oxidation by SOD confirms that hydroxyl radicals act as secondary oxidants formed from superoxide generated by photoexcited nitrate (Fig. S6C).

Superoxide generated by nitrate photoexcitation also oxidized Mn^{2+}(aq) under homogeneous conditions (Fig. S6B). In the presence of SOD, Mn^{2+}(aq) exhibited no oxidation under light exposure, indicating that superoxide drove the oxidation of Mn^{2+}(aq). This result aligns with previous studies reporting Mn^{2+}(aq) oxidation by superoxide formed through nitrate photolysis (Jung et al., 2017a, Jung et al., 2017b, Jung et al., 2024). The superoxide-driven oxidation of Mn^{2+}(aq) further led to the homogeneous nucleation of Mn oxide in solution (Fig. S8). Scanning electron microscopy with energy-dispersive X-ray spectroscopy and ICP-OES analyses revealed that the homogeneously nucleated Mn oxide contained a substantial amount of As, with a Mn-to-As molar ratio of about 1.6:1 (Fig. S8A). XRD analysis showed no distinct diffraction pattern, suggesting that the homogeneously nucleated Mn oxide was likely amorphous (Fig. S8D). Deconvolution of the As 3d XPS spectrum indicated that approximately 55 % of As was present as As(III) and 45 % as As(V) (Fig. S8E). The XPS analysis of the Mn 3s spectrum showed an average Mn oxidation state of approximately +3.1 (Fig. S8F). Overall, these results demonstrate that the photochemical process involving As (III) and Mn^{2+}(aq) enabled indirect homogeneous oxidation to As(V) and Mn(III/IV) via superoxide generated through the photoexcitation of nitrate by UV light under environmentally relevant conditions. Furthermore, this process resulted in the formation of amorphous Mn oxides containing a significant amount of As.

3.4. Heterogeneous photocatalytic oxidation of As(III) and Mn^{2+}(aq) by hematite

While the homogeneous oxidation of As(III) and Mn^{2+}(aq) proceeded exclusively via superoxide, the heterogeneous oxidation on hematite involved multiple pathways. In the presence of SOD, the oxidation of As(III) decreased (Fig. 3A), suggesting that superoxide, generated by the photoexcitation of nitrate in AFW, affects the oxidation of both dissolved and adsorbed As(III). To confirm the role of superoxide in the heterogeneous oxidation of As(III) on hematite, we conducted a control experiment in the absence of Mn^{2+}(aq) under SOD-treated conditions (Fig. S9). A clear decrease in the oxidation of adsorbed As (III) on hematite was observed, confirming that superoxide contributes to the oxidation of surface-bound As(III) on hematite.

To assess the role of hydroxyl radicals in the heterogeneous oxidation of As(III), we used t-BuOH. Strikingly, heterogeneous oxidation of both As(III) and Mn^{2+}(aq) increased in the presence of t-BuOH (Fig. 3C and D). To determine whether this enhancement was due to suppressed hydroxyl radical activity or increased Mn oxide formation, we repeated the experiment without Mn^{2+}(aq) (Fig. S10). The results showed that the heterogeneous oxidation of As(III) slightly decreased, indicating that hydroxyl radicals play only a minor role in its heterogeneous oxidation. Thus, the increased heterogeneous oxidation of As(III) observed in the presence of Mn^{2+}(aq) and t-BuOH suggests that the heterogeneously nucleated Mn oxides played a significant catalytic role in this process (Fig. 3C and D). Previous studies have shown that t-BuOH not only scavenges hydroxyl radicals but also generates peroxyl radicals ($ROO^{\bullet}$), which are highly effective in oxidizing Mn^{2+}(aq) (Gao et al., 2021). The study clearly demonstrated both the formation of $ROO^{\bullet}$ during hydroxyl radicals scavenging by t-BuOH and the subsequent homogeneous oxidation of Mn^{2+}(aq) by $ROO^{\bullet}$. Other studies also reported enhanced photochemical oxidation of Mn^{2+}(aq) when t-BuOH is added as the scavenger of hydroxyl radicals (Jung et al., 2017a, Jung et al., 2021). We can rule out the possibility that the enhanced oxidation of Mn^{2+}(aq) resulted from reaction pathway alteration caused by $^{\bullet}OH$ quenching. While the only remaining homogeneous oxidant of Mn^{2+}(aq) produced from nitrate photolysis except for $ROO^{\bullet}$ is superoxide, as shown in Table S4, superoxide generation is not a competitive pathway relative to the $^{\bullet}OH$-related chain reaction. Therefore, the enhanced oxidation of Mn^{2+}(aq) observed here likely resulted from $ROO^{\bullet}$ formation, promoting the nucleation of Mn oxide on hematite (Gao et al., 2021). The heterogeneously nucleated Mn oxides on hematite then promoted further heterogeneous oxidation of As(III). Collectively, the results suggest that ROS indirectly oxidizes adsorbed As(III), with heterogeneously nucleated Mn oxide acting as a catalytic bridge.

In addition to ROS-mediated mechanisms, we found strong evidence for direct photocatalytic oxidation of As(III) via electron transfer to valence band holes in hematite. This oxidation requires a suitable electron acceptor to capture photoexcited electrons, with molecular oxygen likely serving as the primary acceptor in our system. To evaluate the contribution of this hole-driven pathway, photocatalytic oxidation experiments were conducted under anoxic conditions without Mn^{2+}(aq) (Fig. S11). Under anoxic conditions, As(III) oxidation was markedly suppressed when only As(III) was present, indicating that hole-mediated oxidation is inhibited when electron acceptors (*i.e.*, dissolved oxygen) are unavailable. Combined with previous studies demonstrating the direct photocatalytic oxidation of Mn^{2+}(aq) by hematite, these results underscore the critical role of oxygen in facilitating charge separation and confirm that valence band holes in hematite can directly oxidize adsorbed As(III) and Mn^{2+}(aq) (Jung et al., 2021).

Complexation between Fe(III) and As(III), followed by a photochemical reaction through ligand-to-metal charge transfer (LMCT), is a plausible pathway for the photocatalytic heterogeneous oxidation of As (III) on hematite. Previous studies have shown that photocatalytic oxidation of As(III) by Fe oxides via LMCT leads to photoreduction of Fe (III) to Fe(II) and subsequent release of Fe(II) ions into solution (Bhandari et al., 2011, Xu et al., 2014). In such complexes, electron transfer from the ligand to the central metal ion could lead to the photoreduction of Fe(III) to Fe(II). To evaluate the potential contribution of LMCT in our system, we measured dissolved Fe(II) throughout 6 h of reaction under both oxic and anoxic conditions (Fig. S12A). No detectable dissolved Fe(II) was observed. Considering the likelihood of rapid Fe(II) oxidation, we also monitored H_2O_2 generation, which could be generated during Fe(II) re-oxidation (Fig. S12B). However, H_2O_2 was not detected either. These results suggest that LMCT was likely insignificant under our experimental conditions. Nonetheless, based on previous reports of LMCT-driven As(III) oxidation on Fe oxides and the possibility of rapid Fe(II) adsorption and oxidation on hematite without H_2O_2 formation, we cannot entirely exclude a minor LMCT-mediated contribution to direct photocatalytic electron transfer.

Notably, heterogeneously nucleated Mn oxide on hematite also contributed to As(III) oxidation through a photocorrosion mechanism. Given the distinct adsorption preferences of As(III) and Mn^{2+}(aq) on hematite (Fig. 2), we inferred that As(III) adsorption onto Mn oxides was minimal, rendering direct oxidation of As(III) by Mn oxide less likely. However, based on control experiments with ROS scavengers, increased amounts of heterogeneously nucleated Mn oxide corresponded to a discernible enhancement in the heterogeneous oxidation of As(III) (Figs. 3 and S10). In addition, the lower oxidation state of heterogeneously nucleated Mn oxide (Fig. 1C and E) compared to that observed in the absence of As(III) suggests that the heterogeneously nucleated Mn oxides were reduced by accepting electrons from As(III) under light exposure (Choi et al., 2024, Jung et al., 2021). In the absence of As(III), Mn 3p XPS analysis showed that the ratios of Mn(II), Mn(III) and Mn(IV) were 41, 5, and 54 %, respectively (Fig. S13). However, as clearly shown in the shifted binding energy to a lower level, in the presence of As(III), the photocatalytically nucleated Mn oxide on hematite showed that the ratios of Mn(II), Mn(III) and Mn(IV) were 58, 36, and 6 %, respectively. Accordingly, we infer that electron transfer occurred from adsorbed As (III) to the Mn oxide, potentially mediated by hematite (*i.e.*, photocorrosion).

To further confirm the photocorrosion-driven mechanism, we first photooxidized Mn^{2+}(aq) in the presence of hematite to induce the heterogeneous nucleation of Mn oxide on the hematite surface. After

removing dissolved oxygen by purging with N_2 gas and sealing the reactor, we added As(III) and monitored its oxidation under both light and dark conditions. Interestingly, under light conditions, the heterogeneous oxidation of As(III) was significantly greater than in the dark (Fig. 4A), while the extent of homogeneous oxidation to As(V) remained similar (Fig. 4B). Since the oxidation of As(III) under dark conditions can proceed only via direct electron transfer to Mn oxide, the enhanced heterogeneous oxidation observed under light must result from a photocatalytic process. Furthermore, since hematite alone exhibited negligible photocatalytic activity under anoxic conditions (Fig. S11), the observed greater photocatalytic heterogeneous oxidation of As(III) under light indicates that the heterogeneously nucleated Mn oxide acted as the electron acceptor. Specifically, hematite mediated the photocatalytic oxidation of As(III), while the heterogeneously nucleated Mn oxide accepted photoexcited electrons from hematite via a photocorrosion process. Meanwhile, the reduced Mn oxide is likely re-oxidized by the photocatalytic activity of hematite. Although the heterogeneously nucleated Mn oxide undergoes reduction by accepting photoexcited electrons, the Mn(III) equivalent continued to increase (Fig. 1B), suggesting that both photocorrosion and photocatalytic re-activation of Mn oxide occurred.

Overall, we demonstrated the simultaneous oxidation of As(III) and Mn^{2+}(aq) in the presence of hematite through both homogeneous and heterogeneous photochemical processes (Fig. 4C). Homogeneous photochemical oxidation occurred via ROS generated from nitrate photolysis. Heterogeneous photocatalytic oxidation of As(III) proceeds via multiple mechanisms: (1) ROS-mediated oxidation, including contributions from superoxide and hydroxyl radicals; (2) direct photocatalytic electron transfer with oxygen as the electron acceptor and with photocorrosion by heterogeneously nucleated Mn oxides. Among these pathways, direct photocatalytic electron transfer pathways, facilitated by either oxygen or Mn oxide, accounted for more than 60 % of the total As(III) oxidation, as evidenced by the greater suppression of As(III) oxidation under conditions that inhibit direct electron transfer (Figs. 3, 4, S11, and S14).

Although ROS generation and direct electron transfer are well-established pathways in semiconductor photocatalysis, our results reveal previously unrecognized ternary interactions among Fe oxide, As (III), and Mn^{2+}(aq) under sunlight. Contrary to the prevailing view that As(III) oxidation proceeds primarily via direct electron transfer accompanied by the reduction of Mn oxide, we show the concurrent photocatalytic oxidation of both As(III) and Mn^{2+}(aq) by hematite. Moreover, the heterogeneously nucleated Mn oxide on hematite, formed through the photocatalytic oxidation of Mn^{2+}(aq), plays a significant role in As (III) oxidation via a photocorrosion process.

Given the frequent co-occurrence of Fe oxide, As, and Mn in As-

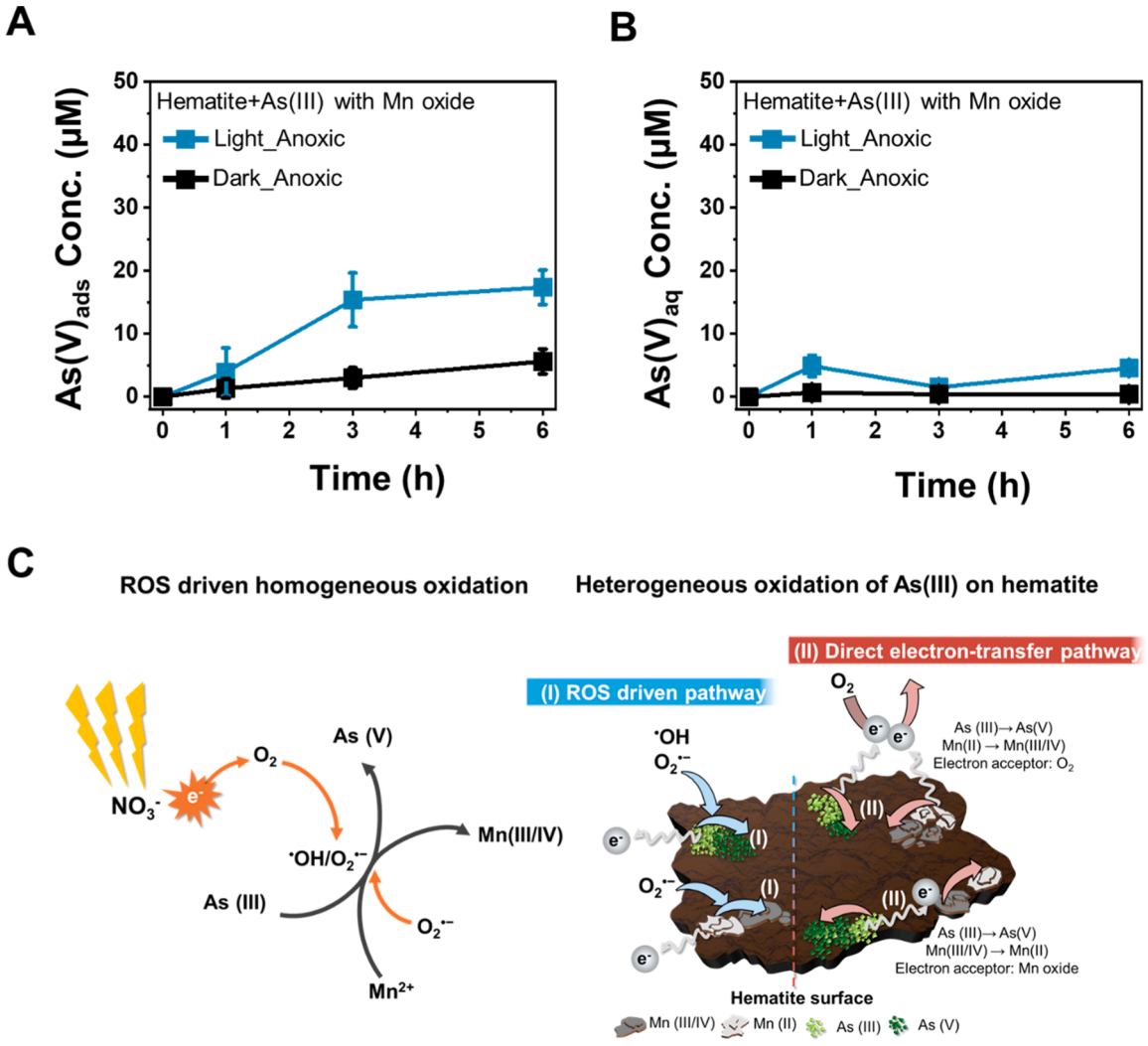

Fig. 4. Photocatalytic oxidation of As(III) facilitated by the heterogeneously nucleated Mn oxide on hematite via a photocorrosion pathway. (A and B) Heterogeneous and homogeneous photocatalytic oxidation of As(III) under anoxic conditions in the presence of hematite and Mn oxide heterogeneously nucleated on hematite through photocatalytic oxidation. (C) Schematic diagram of the simultaneous oxidation of As(III) and Mn^{2+}(aq) in the presence of hematite under light exposure.

contaminated systems, our findings highlight the importance of understanding Fe–As–Mn ternary interactions for predicting the fate and transport of As species and for improving remediation strategies for As-contaminated surface waters. Future studies should further elucidate the molecular-level interactions in Fe–As–Mn ternary systems using extended X-ray absorption fine structure analyses, density functional theory simulations, and electrochemical approaches. In addition, quantitative characterization of photochemical pathways using electron paramagnetic resonance spectroscopy and quantum yield analysis is warranted.

3.5. *Natural sunlight-driven simultaneous photochemical oxidation of As (III) and Mn^{2+}(aq) in the presence of hematite*

Based on the experimental results and the frequent co-occurrence of Fe, As, and Mn in As-contaminated surface water systems, we infer that the sunlight-driven photochemical oxidation pathway observed in this study is environmentally plausible. However, given the significant role of homogeneous oxidation of As(III) and Mn^{2+}(aq) via UV-driven photoexcitation of nitrate, the higher UV intensity of the Xe-lamp likely led to an overestimation of As(III) oxidation compared to that under natural sunlight, which exhibits lower UV irradiance. In particular, nitrate photoexcitation occurs at near 305 nm (Jung et al., 2017a), a wavelength that is largely absent in natural sunlight compared with the Xe-lamp (Fig. S15).

To assess the role of visible light, we conducted experiments using a 400 nm cutoff filter to block UV radiation. The results indicate that the direct heterogeneous oxidation of As(III), coupled with the photocorrosion of Mn oxide, is the most effective oxidation pathway (Fig. S16). Under the 400 nm cutoff, As(III) adsorption on hematite remained consistent regardless of the presence of Mn^{2+}(aq) (Fig. S16A), and total As(V) concentrations were similar in both systems (Fig. S16B). Interestingly, the heterogeneous oxidation of As(III) was greater in the presence of Mn^{2+}(aq), whereas the homogeneous oxidation was greater in its absence (Fig. S16C and S16D). These results contrast with those observed under full-spectrum Xe-lamp conditions, where both the homogeneous and heterogeneous oxidation of As(III) were greater in the absence of Mn^{2+}(aq) (Fig. S2). The increased heterogeneous oxidation of

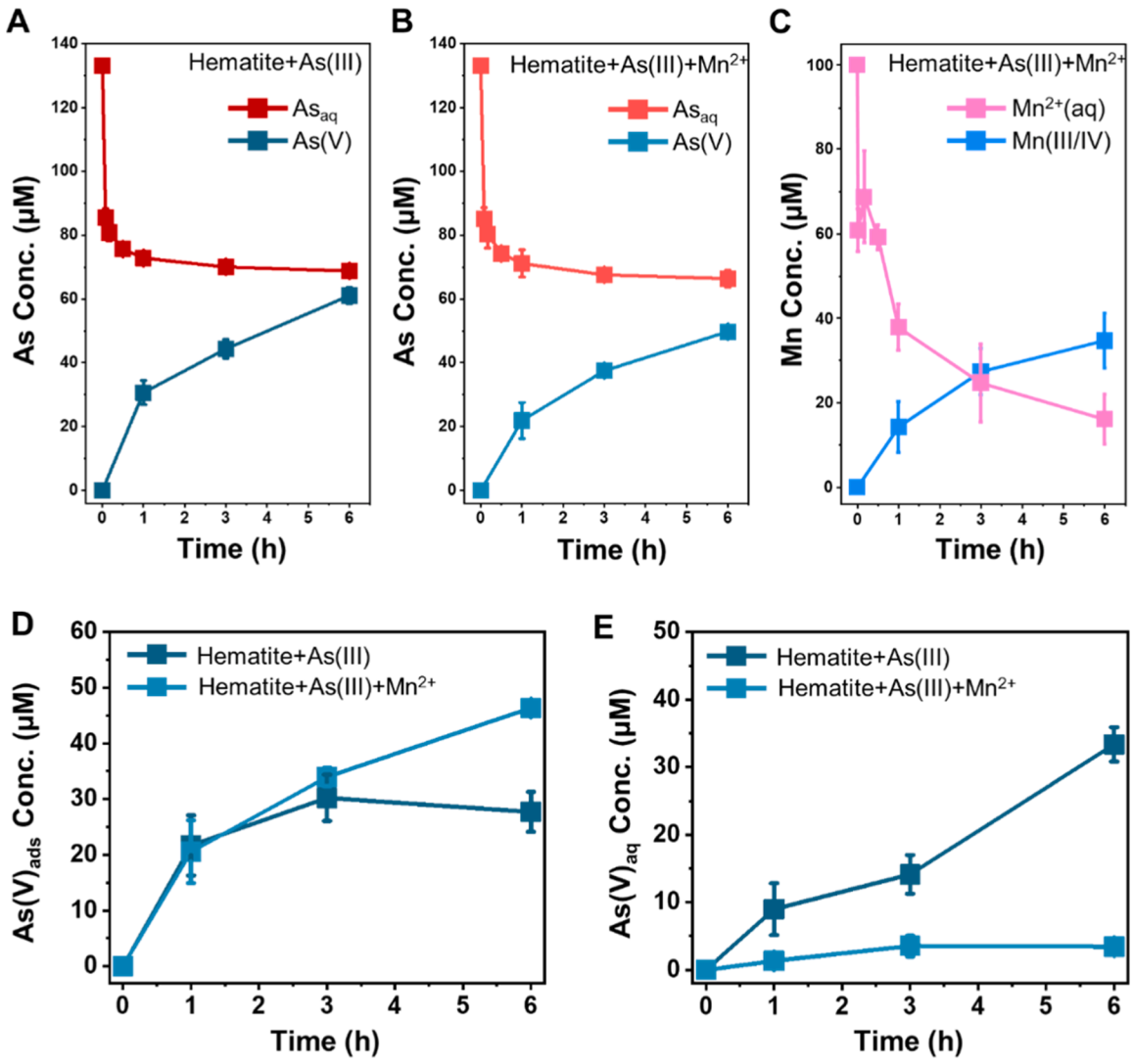

Fig. 5. Natural sunlight-driven simultaneous photochemical oxidation of As(III) and Mn^{2+}(aq) by hematite. (A) Concentrations of As species during the photochemical reaction in the presence of only As(III) and hematite. (B and C) Concentrations of As and Mn species in the presence of both As(III) and Mn^{2+}(aq). (D and E) Comparison of the adsorbed As(V) on hematite and aqueous As(V) following the photochemical oxidation of As(III) and Mn^{2+}(aq) by hematite. Under Xe-lamp exposure, both aqueous and adsorbed As(III) were oxidized more extensively (Fig. S2). Under natural sunlight, however, the presence of Mn^{2+}(aq) promoted greater heterogeneous oxidation of As(III) than the system containing only As(III). This trend corresponds with our Xe-lamp experiments using a 400 nm cutoff filter. We infer that under sunlight, heterogeneously nucleated Mn oxide plays a crucial role in the photocatalytic oxidation of adsorbed As(III) on hematite via the photocorrosion-driven pathway of the heterogeneously nucleated Mn oxide.

As(III) in the presence of Mn^{2+}(aq) under visible light suggests that the photocorrosion of Mn oxide is the primary mechanism driving the heterogeneous oxidation of As(III) under environmentally relevant conditions (Fig. S16D). In addition, in the presence of Mn^{2+}(aq), the heterogeneous photocatalytic oxidation of As(III) remained consistent regardless of the presence of the UV cutoff filter (Fig. S17A). In contrast, the homogeneous oxidation of As(III) was lower when the UV cutoff filter was applied (Fig. S17B). This result indicates that UV light has an insignificant effect on the heterogeneous photocatalytic oxidation of As (III), whereas homogeneous As(III) oxidation decreases due to the reduced nitrate photolysis and corresponding decline in superoxide generation under the UV cutoff.

Outdoor experiments under natural sunlight further confirmed this trend. The heterogeneous oxidation of As(III) was more pronounced in the presence of Mn^{2+}(aq) (Fig. 5), and As(III) adsorption on hematite under sunlight was consistent with the Xe-lamp experiments (Fig. 5A and 5B), with aqueous As concentrations of 68.8 ± 1.3 μM and 66.4 ± 2.6 μM in the presence and absence of Mn^{2+}(aq), respectively. Although total As(III) oxidation was higher in the absence of Mn^{2+}(aq) (Fig. 5A and B), heterogeneous oxidation was greater when Mn^{2+}(aq) was present (Fig. 5D and 5E). These findings confirm that the heterogeneously nucleated Mn oxides on hematite promote the photocatalytic oxidation of As(III) via a photocorrosion mechanism. In environments where As (III), Mn^{2+}(aq), and Fe oxides coexist, sunlight exposure can thus drive the simultaneous oxidation of Mn^{2+}(aq) and As(III). Specifically, the photocatalytic oxidation of Mn^{2+}(aq) on hematite induces Mn oxide nucleation, which subsequently serves as an electron sink that facilitates the direct oxidation of As(III) to As(V). In addition to heterogeneous oxidation, substantial homogeneous oxidation of As(III) occurred under sunlight in the absence of Mn^{2+}(aq) (Fig. 5E). This result demonstrates that photochemical homogeneous oxidation of As(III) driven by photoexcitation of environmental substances such as nitrate in surface water systems can proceed significantly even under the weak UV intensity reaching the Earth's surface, highlighting its potential contribution to As (III) oxidation in natural surface waters.

Notably, As adsorption remained consistent across all experimental conditions. Regardless of Mn^{2+}(aq) presence or light exposure, hematite adsorbed similar amounts of As. Although Mn^{2+}(aq) oxidation was approximately twice as high in outdoor tests compared to that in Xe-lamp experiments, attributable to the larger light exposure area of the outdoor reactor (Figs. 1B and 5C) (Choi et al., 2024, Jung et al., 2021), the adsorption of As on hematite showed no significant change. The results also indicate that the adsorption of As onto heterogeneously nucleated Mn oxide is minimal, and that As and Mn(II) occupy distinct adsorption sites on hematite. Overall, the outdoor experiments demonstrated that simultaneous photocatalytic oxidation of As(III) and Mn^{2+}(aq) by hematite is an environmentally plausible process. The direct electron transfer from adsorbed As(III) to hematite, facilitated by the photocorrosion of Mn oxide, played a crucial role in the heterogeneous oxidation of As(III).

4. Conclusions

While previous studies have primarily focused on binary interactions (*e.g.*, Fe–As, Fe–Mn, and Mn–As), our work elucidates the complex ternary interactions among hematite, As, and Mn under light-exposed conditions. These findings provide a novel framework for future research incorporating additional environmental constituents to better understand the fate and transport of As in natural aqueous systems. In addition to advancing the fundamental understanding of redox interactions among hematite, As(III), and Mn^{2+}(aq) under environmentally relevant conditions, our results could provide a novel photocatalytic approach for remediating As-contaminated surface water. Although the oxidation rate of Mn^{2+}(aq) is typically slow, the hematite-driven photocatalytic process demonstrated in this study enabled rapid Mn^{2+}(aq) oxidation and subsequent immobilization via heterogeneous nucleation of Mn oxide, even in the co-presence of As (III). The comparable or greater As(III) adsorption capacity of hematite relative to other adsorbents (Table S5), combined with its ability to host distinct adsorption sites for As(III) and Mn^{2+}(aq), further highlights its potential for engineering applications in environments contaminated with both As and Mn.

Because sunlight is ubiquitous in surface waters, rapid and concurrent heterogeneous oxidation of As(III) and Mn^{2+}(aq) by hematite would be an environmentally and economically viable approach for As-contaminated systems. Notably, in the presence of Mn^{2+}(aq), heterogeneous pathways accounted for more than 90 % of As(V) formation under natural sunlight (Fig. S18). Visible-light-driven heterogeneous oxidation by the photocorrosion of Mn oxide therefore represents an efficient pathway not only for contaminant immobilization on hematite but also for metal resource recovery. In addition, because our study elucidates the fundamental oxidation pathways of both homogeneous and heterogeneous processes in the ternary system, the results may also inform the development of engineered remediation strategies using artificial light sources such as Xe-lamps and mercury lamps.

Data availability

Data will be made available on request.

CRediT authorship contribution statement

Junyeong Choi: Writing – review & editing, Writing – original draft, Visualization, Validation, Software, Methodology, Investigation, Formal analysis, Data curation, Conceptualization. **Donggeun Kim:** Writing – original draft, Visualization, Data curation. **Seung Soo Steve Lee:** Formal analysis, Data curation. **John D. Fortner:** Methodology, Investigation, Data curation. **Yoon Myung:** Formal analysis, Data curation. **Yuanzhi Tang:** Writing – review & editing, Writing – original draft, Supervision, Conceptualization. **Haesung Jung:** Writing – review & editing, Writing – original draft, Supervision, Project administration, Investigation, Funding acquisition, Conceptualization.

Declaration of competing interest

The authors declare that they have no known competing financial interests or personal relationships that could have appeared to influence the work reported in this paper.

Acknowledgments

This work was supported by the National Research Foundation of Korea (NRF) grant funded by the Korea government (MSIT) (Grant No. RS2025-23525246), and the Global-Learning & Academic Research Institution for Master's and PhD students and Postdocs (LAMP) Program of the National Research Foundation of Korea (NRF) funded by the Ministry of Education (Grant no. RS2024-00444460). Y. Tang acknowledges funding support from the U.S. National Science Foundation (NSF) (Grant No. 2108688) and National Aeronautics and Space Administration (NASA) (Grant No. 80NSSC21K0483). The use of synchrotron-based XAS was supported by beamline 7D at the Pohang Light Source-II, Pohang Accelerating Laboratory.

Supplementary materials

Supplementary material associated with this article can be found, in the online version, at doi:10.1016/j.watres.2025.125182.

References

Abedin, M.J., Cotter-Howells, J., Meharg, A.A., 2002. Arsenic uptake and accumulation in rice (Oryza sativa L.) irrigated with contaminated water. Plant Soil 240 (2), 311–319.

Ayotte, J.D., Medalie, L., Qi, S.L., Backer, L.C., Nolan, B.T., 2017. Estimating the High-Arsenic Domestic-Well Population in the Conterminous United States. Environ. Sci. Technol. 51 (21), 12443–12454.

Bai, J., Yuan, Z., Su, X., 2024. Spatiotemporal distribution patterns of iron, manganese, and arsenic within the river infiltration zone and the potential geochemical activity at key interfaces. Appl. Geochem. 172, 106123.

Bednar, A.J., Garbarino, J.R., Burkhardt, M.R., Ranville, J.F., Wildeman, T.R., 2004. Field and laboratory arsenic speciation methods and their application to natural-water analysis. Water Res. 38 (2), 355–364.

Bhandari, N., Reeder, R.J., Strongin, D.R., 2011. Photoinduced Oxidation of Arsenite to Arsenate on Ferrihydrite. Environ. Sci. Technol. 45 (7), 2783–2789.

Choi, J., Choi, W., Hwang, H., Tang, Y., Jung, H., 2024. Natural sunlight-driven oxidation of Mn2+(aq) and heterogeneous formation of Mn oxides on hematite. Chemosphere 348, 140734.

Chowdhury, T.R., Basu, G.K., Mandal, B.K., Biswas, B.K., Samanta, G., Chowdhury, U.K., Chanda, C.R., Lodh, D., Roy, S.L., Saha, K.C., Roy, S., Kabir, S., Quamruzzaman, Q., Chakraborti, D., 1999. Arsenic poisoning in the Ganges delta. Nature 401 (6753), 545–546.

Cornell, R.M., Schwertmann, U., 2003. The iron oxides: structure, properties, reactions, occurrences, and uses. Wiley-VCH, Weinheim.

Diem, D., Stumm, W., 1984. Is dissolved Mn2+ being oxidized by O2 in absence of Mn-bacteria or surface catalysts? Geochim. Cosmochim. Acta 48 (7), 1571–1573.

Eisenberg, G., 1943. Colorimetric Determination of Hydrogen Peroxide. Ind. Eng. Chem., Anal. Ed. 15 (5), 327–328.

Ferris, F.G., Phoenix, V., Fujita, Y., Smith, R.W., 2004. Kinetics of calcite precipitation induced by ureolytic bacteria at 10 to 20°C in artificial groundwater. Geochim. Cosmochim. Acta 68 (8), 1701–1710.

Gao, Z., Zhang, D., Jun, Y.-S., 2021. Does Tert-Butyl Alcohol Really Terminate the Oxidative Activity of •OH in Inorganic Redox Chemistry? Environ. Sci. Technol. 55 (15), 10442–10450.

Gude, J.C.J., Rietveld, L.C., van Halem, D., 2017. As(III) oxidation by MnO(2) during groundwater treatment. Water Res. 111, 41–51.

Herath, I., Vithanage, M., Bundschuh, J., Maity, J.P., Bhattacharya, P., 2016. Natural Arsenic in Global Groundwaters: Distribution and Geochemical Triggers for Mobilization. Curr. Pollut. Rep. 2 (1), 68–89.

Hjorth, T., 2004. Effects of freeze-drying on partitioning patterns of major elements and trace metals in lake sediments. Anal. Chim. Acta 526 (1), 95–102.

Jung, H., Chadha, T., Kim, D., Biswas, P., Jun, Y.-S., 2017a. Photochemically-assisted Fast Abiotic Oxidation of Manganese and Formation of δ–MnO_2 Nanosheets in Nitrate Solution. Chem. Commun. 53, 4445–4448.

Jung, H., Chadha, T.S., Min, Y., Biswas, P., Jun, Y.-S., 2017b. Photochemically-Assisted Synthesis of Birnessite Nanosheets and Their Structural Alteration in the Presence of Pyrophosphate. ACS Sustain. Chem. Eng. 5 (11), 10624–10632.

Jung, H., Lee, B., Kim, D., Gao, Z., Chou, P.-I., Jun, Y.-S., 2024. Three Distinctive Steps for Heterogeneous Nucleation of Tunnel-Structured Mn Oxide on Quartz under Light Exposure. Environ. Sci. Technol. 58 (48), 21200–21209.

Jung, H., Xu, X., Wan, B., Wang, Q., Borkiewicz, O.J., Li, Y., Chen, H., Lu, A., Tang, Y., 2021. Photocatalytic oxidation of dissolved Mn(II) on natural iron oxide minerals. Geochim. Cosmochim. Acta 312, 343–356.

Kim, D.-H., Lee, J., Ryu, J., Kim, K., Choi, W., 2014. Arsenite Oxidation Initiated by the UV Photolysis of Nitrite and Nitrate. Environ. Sci. Technol. 48 (7), 4030–4037.

Lenoble, V., Deluchat, V., Serpaud, B., Bollinger, J.-C., 2003. Arsenite oxidation and arsenate determination by the molybdene blue method. Talanta 61 (3), 267–276.

Liu, L., Guo, D., Ning, Z., Liu, C., Qiu, G., 2021. Solar irradiation induced oxidation and adsorption of arsenite on natural pyrite. Water Res. 203, 117545.

Liu, L., Zhang, M., Suib, S.L., Qiu, G., 2022. Rapid photooxidation and removal of As(III) from drinking water using Fe-Mn composite oxide. Water Res. 226, 119297.

Lombard, M.A., Daniel, J., Jeddy, Z., Hay, L.E., Ayotte, J.D., 2021. Assessing the Impact of Drought on Arsenic Exposure from Private Domestic Wells in the Conterminous United States. Environ. Sci. Technol. 55 (3), 1822–1831.

Mandal, B.K., Suzuki, K.T., 2002. Arsenic round the world: a review. Talanta 58 (1), 201–235.

Manning, B.A., Fendorf, S.E., Bostick, B., Suarez, D.L., 2002. Arsenic(III) Oxidation and Arsenic(V) Adsorption Reactions on Synthetic Birnessite. Environ. Sci. Technol. 36 (5), 976–981.

Manning, B.A., Goldberg, S., 1997. Adsorption and Stability of Arsenic(III) at the Clay Mineral−Water Interface. Environ. Sci. Technol. 31 (7), 2005–2011.

Mondal, D., Banerjee, M., Kundu, M., Banerjee, N., Bhattacharya, U., Giri, A.K., Ganguli, B., Sen Roy, S., Polya, D.A., 2010. Comparison of drinking water, raw rice and cooking of rice as arsenic exposure routes in three contrasting areas of West Bengal, India. Environ. Geochem. Health. 32 (6), 463–477.

Morgan, J.J., 2005. Kinetics of reaction between O2 and Mn(II) species in aqueous solutions. Geochim. Cosmochim. Acta 69 (1), 35–48.

Nickson, R., McArthur, J., Burgess, W., Ahmed, K.M., Ravenscroft, P., Rahman, M., 1998. Arsenic poisoning of Bangladesh groundwater. Nature 395 (6700), 338-338.

Nickson, R.T., McArthur, J.M., Ravenscroft, P., Burgess, W.G., Ahmed, K.M., 2000. Mechanism of arsenic release to groundwater, Bangladesh and West Bengal. Appl. Geochem. 15 (4), 403–413.

Notini, L., ThomasArrigo, L.K., Kaegi, R., Kretzschmar, R., 2022. Coexisting Goethite Promotes Fe(II)-Catalyzed Transformation of Ferrihydrite to Goethite. Environ. Sci. Technol. 56 (17), 12723–12733.

Organization, W.H., 2022. Guidelines for drinking-water quality: incorporating the first and second addenda. World Health Organization, Geneva.

Pi, K., Xie, X., Sun, S., Van Cappellen, P., Xiao, Z., Zhang, D., Wang, Y., 2024. Arsenic redox disequilibrium in geogenic contaminated groundwater: Bioenergetic insights from organic molecular characterization and gene-informed modeling. Water Res. 267, 122459.

Ramsay, L., Petersen, M.M., Hansen, B., Schullehner, J., van der Wens, P., Voutchkova, D., Kristiansen, S.M., 2021. Drinking Water Criteria for Arsenic in High-Income, Low-Dose Countries: The Effect of Legislation on Public Health. Environ. Sci. Technol. 55 (6), 3483–3493.

Ryu, J., Monllor-Satoca, D., Kim, D.-h., Yeo, J., Choi, W., 2013. Photooxidation of Arsenite under 254 nm Irradiation with a Quantum Yield Higher than Unity. Environ. Sci. Technol. 47 (16), 9381–9387.

Schwertmann, U., Friedl, J., Stanjek, H., 1999. From Fe(III) Ions to Ferrihydrite and then to Hematite. J. Colloid Interface Sci. 209 (1), 215–223.

Takahashi, Y., Minamikawa, R., Hattori, K.H., Kurishima, K., Kihou, N., Yuita, K., 2004. Arsenic Behavior in Paddy Fields during the Cycle of Flooded and Non-flooded Periods. Environ. Sci. Technol. 38 (4), 1038–1044.

Tebo, B.M., Clement, B.G., Dick, G.J., 2007. Biotransformations of manganese. In: Hurst, C.J., Knudsen, G.R., McInerney, M.J., Stetzenbach, L.D., Walter, M.V. (Eds.), Manual of Environmental Microbiology. ASM Press, Washington, DC, pp. 1223–1238.

Winkel, L.H.E., Trang, P.T.K., Lan, V.M., Stengel, C., Amini, M., Ha, N.T., Viet, P.H., Berg, M., 2011. Arsenic pollution of groundwater in Vietnam exacerbated by deep aquifer exploitation for more than a century. Proc. Natl. Acad. Sci. U.S.A. 108 (4), 1246–1251.

Xu, J., Li, J., Wu, F., Zhang, Y., 2014. Rapid Photooxidation of As(III) through Surface Complexation with Nascent Colloidal Ferric Hydroxide. Environ. Sci. Technol. 48 (1), 272–278.

Zhang, G., Qu, J., Liu, H., Liu, R., Wu, R., 2007. Preparation and evaluation of a novel Fe-Mn binary oxide adsorbent for effective arsenite removal. Water Res. 41 (9), 1921–1928.

Zhou, Y., Zeng, Y., Zhou, J., Guo, H., Li, Q., Jia, R., Chen, Y., Zhao, J., 2017. Distribution of groundwater arsenic in Xinjiang, P.R. China. Appl. Geochem 77, 116–125.

Zhu, M., Paul, K.W., Kubicki, J.D., Sparks, D.L., 2009. Quantum Chemical Study of Arsenic (III, V) Adsorption on Mn-Oxides: Implications for Arsenic(III) Oxidation. Environ. Sci. Technol. 43 (17), 6655–6661.